2026 IEEE/SICE International Symposium on System Integration (SII)
January 11-14, 2026. Cancún, México

Fuzzy-Adaptive Force-Compliant Control and Sensorless Estimation of a Hybrid Aerial Manipulator for Contact-Based Pipeline Repair

Ezeldin N. Moustafa, Mitsuhiro Kamezaki, *Member, IEEE*, Shota Miyake, and Shigeki Sugano, *Fellow, IEEE*

***Abstract*— Aerial manipulators offer a compelling solution for maintenance tasks in hazardous or hard-to-reach environments. Contact-based operations, such as pipeline crack repair, demand not only precise trajectory tracking but also stable and controlled force application when interacting with cylindrical surfaces subject to friction. These dual objectives are challenging due to the aerial system's inherent instability, strong nonlinearities, and sensitivity to disturbances. While impedance control enables direct interaction, it replaces the position control loop that can reduce robustness under dynamic conditions. In contrast, conventional admittance control wraps around existing loops but suffers from limited adaptability and challenging gain tuning. This paper proposes a unified force-compliant control framework for a quadrotor equipped with a hybrid manipulator. An adaptive backstepping–adaptive fast terminal sliding mode controller (AB–AFTSMC) governs the inner trajectory loop, ensuring reliable tracking performance. Over this structure, a fuzzy-admittance outer loop modulates the desired reference trajectories based on desired force, enabling compliant interaction during contact without altering the underlying control architecture. Interaction forces are estimated using a lightweight disturbance observer (DOB), enabling low-computation, sensorless feedback without the weight or complexity of force sensors. Validation is carried out in MATLAB Simscape through a 3D physics-based model. The results demonstrate reliable tracking, compliant force build-up, and consistent free-flight-to-contact transitions.**

I. Introduction

Unmanned Aerial Vehicles (UAVs) are increasingly deployed in hazardous or hard-to-reach environments to perform tasks such as infrastructure inspection, environmental monitoring, and surveillance [1], [2]. Although advances in onboard sensing and autonomy have expanded their capabilities, most UAV systems remain limited to passive observation, focusing on data collection rather than direct physical interaction with the environment [3].

To overcome this limitation, Unmanned Aerial Manipulators (UAMs) combine the agility of UAVs with the manipulation capabilities of robotic arms, enabling active physical interaction. They have been used for object grasping [4], aerial screwing [5], and 3D printing [6]. Their effectiveness in elevated or constrained environments makes them ideal for inspection and maintenance, reducing cost, time, and risk. Demonstrated applications include structural evaluation [7] and contact-based inspection [8].

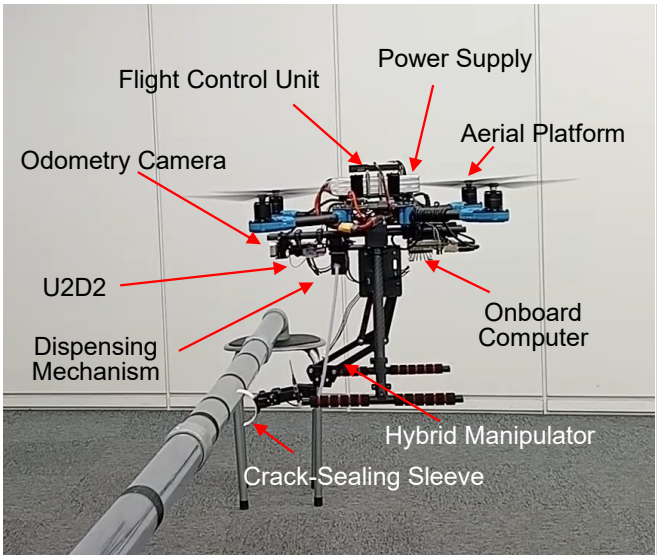

Fig. 1. The developed system combines a Holybro X500 V2 quadrotor with a 3-DOF hybrid manipulator for contact-based pipeline repair.

Pipeline crack repair requires precise intervention in hard-to-access environments to prevent leakage and ensure structural safety. The system in Fig. 1 employs a 3-DOF hybrid parallelogram-based manipulator that combines serial and parallel structural features, achieving a balance between reach and stability while minimizing inertia by positioning actuators near the UAV's center of gravity (CoG). Its architecture decouples orientation from position control, and a dual-tool end-effector enables sequential adhesive dispensing and sleeve sealing [9], providing a weld-free and structurally reliable solution for aerial use. Prior aerial repair approaches using polyurethane foam with delta-type manipulators [10] faced limited access to underside cracks and reduced sealing reliability. Recently, sleeve-based repair using a quadrotor with a 2-DOF manipulator was demonstrated in [11], but its teleoperated setup and cascaded PID control constrained autonomy and robustness. The absence of interaction force regulation during sleeve installation further highlights the need for a compliant, force-aware control framework, motivating the unified approach proposed in this study.

This work was supported in part by the Research Institute of Science and Engineering and the Future Robotics Organization, Waseda University. (Corresponding author: Ezeldin N. Moustafa) ezeldin-moustafa@akane.waseda.jp

E. N. Moustafa is with the Graduate School of Creative Science and Engineering, Waseda University, Tokyo, Japan.

M. Kamezaki is with the Graduate School of Engineering, The University of Tokyo, Japan, and with the Future Robotics Organization, Waseda Univ.

S. Miyake is with the Future Robotics Organization, Waseda Univ. and with the Graduate School of Engineering Science, The University of Osaka, Japan.

S. Sugano is with the Department of Modern Mechanical Engineering, Waseda University, Tokyo, Japan.

978-1-6654-5784-2/26/$31.00 ©2026 IEEE

Achieving stable and precise control during physical interaction remains highly challenging due to the nonlinear nature of UAM dynamics and their high sensitivity to external disturbances [12]. While impedance control allows direct modulation of interaction dynamics, it typically overrides the position control loop and may reduce overall tracking robustness. In contrast, conventional admittance control preserves the original controller structure but often exhibits limited adaptability and sensitivity to gain tuning [13].

To achieve compliant sleeve installation on curved pipe surfaces, this work introduces a robust control framework. A fuzzy-admittance outer loop adapts the desired motion commands, shaping position based on contact force error and UAV pitch angle, while the inner loop applies adaptive backstepping (AB) for translational motion and adaptive fast terminal sliding mode control (AFTSMC) for attitude and joint regulation. In this cooperative scheme, joint θ_3 compensates for pitch-induced orientation shifts to maintain sleeve alignment, while joints θ_1 and θ_2 maintain precise contact with the crack.

A low-complexity disturbance observer (DOB) estimates external forces in real time using filtered model-based and measured accelerations. This sensorless approach facilitates compliant, contact-based operation without force sensors, keeping the framework compact, modular, and suitable for onboard pipeline repair.

The main contributions of this paper are as follows:

1) Propose a fuzzy-admittance-based compliant force control strategy for underactuated aerial manipulators, where contact force error and UAV pitch angle modulate virtual trajectory commands to produce smooth, adaptive contact forces through UAV inclination. The cooperative control structure allows the manipulator to compensate for orientation changes and maintain task-space accuracy during contact.
2) Present a unified control architecture that combines the AB–AFTSMC inner loop for position, attitude, and joint regulation with the fuzzy-admittance outer loop for compliant force adaptation. This integrated framework achieves robust trajectory tracking and adaptive interaction during contact tasks.
3) Incorporate a lightweight, sensorless DOB-based force estimation scheme to provide real-time contact force feedback without additional sensors, supporting compliant force control in dynamic contact scenarios involving friction and impact.

II. Related Work

This section reviews existing studies on force control strategies for aerial manipulators. A fully actuated hexarotor was proposed in [14] to achieve arbitrary pose control of the aerial base during contact-based inspection of complex surfaces using impedance control. While this approach enhanced contact stability, it came at the cost of increased mechanical complexity and power consumption. By contrast, the underactuated quadrotor offered structural simplicity but suffered from strong dynamic coupling; for instance, forward motion inherently required attitude changes such as pitching [15]. A combined pose–wrench control framework was presented in [16], where a quadrotor was modeled as a wrench generator to achieve hybrid pose and force control during direct contact with the environment. This approach demonstrated the feasibility of coordinating position and interaction force regulation but was limited to offline input mapping rather than real-time adaptation. In [17], a quadrotor with a 1-DOF overhead arm was applied to sensor deployment, yet the lack of closed-loop attitude regulation caused instability under high-force interactions at steep pitch angles, limiting task effectiveness. Similarly, [18] generated contact force on vertical walls through thrust–attitude coupling with feedback from an environment-mounted force/torque sensor, but reliance on external sensing and a static contact assumption restricted autonomy and applicability to dynamic tasks.

For force estimation, [19] employed a combination of two DOBs and a recursive least squares (RLS) scheme to identify environmental dynamics. While effective, this approach required running two parallel DOBs alongside the RLS estimator, which increased computational complexity and reduced suitability for aerial platforms. An unscented Kalman filter approach was proposed in [20] for estimating external forces and torques acting on quadrotors. This method explicitly accounted for sensor noise characteristics within the estimation process. However, the results exhibited overshoot in the estimated wrench, which was undesirable when the estimate was employed for feedback control. In [21], force estimation was performed using DOB-based linearization combined with fast transversal recursive least squares (FTRLS) as an adaptive estimator. While effective in simulation, its reliance on careful parameter tuning and relatively high computational load posed challenges for real-time deployment on UAVs with limited onboard processing.

To improve trajectory tracking in UAMs, various robust and nonlinear control strategies were proposed. Model predictive control (MPC) with differential dynamic programming (DDP) [22] handled planning under constraints but relied on model simplifications, reducing robustness to uncertainties. Adaptive sliding mode control (ASMC) [23] enhanced robustness but suffered from chattering due to discontinuous control laws. Finite-time adaptive observers with prescribed performance [24] and adaptive prescribed performance control (APPC) [25] improved convergence but introduced high computational cost, delayed observer response, and tuning sensitivity. Low-complexity controllers with prescribed performance [26] offered improved real-time feasibility but degraded under fast dynamics. These methods traded off robustness, complexity, and convergence speed.

In this work, a unified force-compliant control strategy is presented for a quadrotor with a hybrid manipulator to achieve robust trajectory tracking and stable contact force during pipeline repair. A fuzzy-admittance outer loop modulates the desired motion based on contact force error and UAV pitch angle, promoting compliant interaction through inclination-induced force. Joint θ_3 compensates for pitch-induced orientation changes, while θ_1 and θ_2 maintain con-

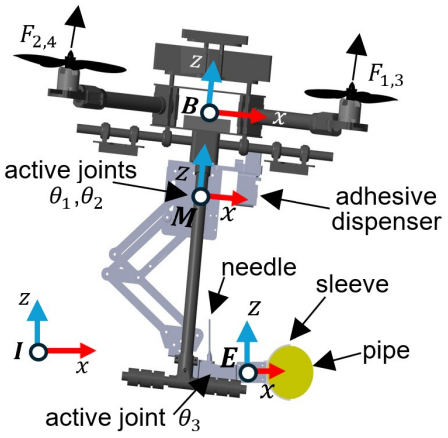

Fig. 2. Coordinate frames (I, B, M, E), active joints, and integrated repair mechanisms (sleeve installation and adhesive dispensing) of the UAM.

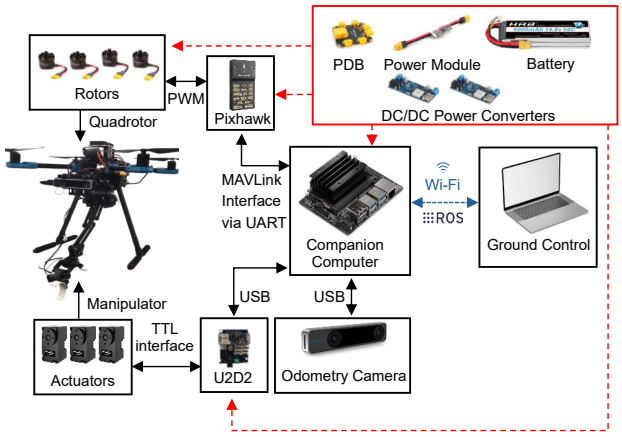

Fig. 3. Overview of system integration encompassing both hardware and software components.

tact precision. An AB–AFTSMC governs position, attitude, and joint control, with a lightweight DOB providing real-time, sensorless force estimation. Simscape-based validation illustrates accurate tracking, smooth force buildup, and controlled pitch recovery before sleeve release, highlighting the effectiveness of the proposed approach for aerial contact with complex surfaces.

III. System Description

This section presents the description and integration of the aerial platform with the developed manipulator.

A. Aerial Platform

The aerial platform is based on a customized Holybro X500 V2 quadrotor with a 500 mm wheelbase, as shown in Fig.1. The platform was chosen for its modular design, and payload capacity of up to 1.5 kg (including battery) [27].

B. Manipulator Design

This subsection presents the design and functionality of the manipulator with a dual-tool end-effector.

1) Manipulator Structure: The developed 3-DOF hybrid manipulator, shown in Fig. 2, integrates a parallelogram-based mechanism for planar motion with a serial orientation joint. Joints θ_1 and θ_2 drive the main parallelogram while auxiliary parallelograms mechanically decouple the end-effector orientation and enhance structural rigidity. Joint θ_3 controls end-effector rotation, enabling independent alignment with surface cracks. A dual-tool end-effector with the tools arranged perpendicularly to facilitate sequential tasks such as adhesive dispensing followed by sleeve application, without requiring landing or manual reconfiguration.

The design features base-mounted actuators to minimize moving mass and improve flight stability. By mechanically decoupling position and orientation control, the structure simplifies kinematic computation, improves orientation accuracy, and offers a compact, high-coverage workspace well suited for operation in confined pipeline environments.

The manipulator is 3D-printed in ABS and actuated by Dynamixel XC330-M288-T motors with a maximum torque of 0.93 Nm at 5 V and 1.8 A [28]. Bearings are used for the passive joints. During flight, the arm folds into a compact form to reduce drag, volume, and shift the CoG closer to the UAV's center, enhancing stability and efficiency.

2) Repairing Mechanisms and Dual-Tool End-Effector: The end-effector features two orthogonally mounted tools controlled by joint θ_3, enabling task-phase-dependent switching between adhesive dispensing and sleeve installation using a single actuator as shown in Fig. 2. The adhesive dispenser consists of a syringe mounted at the base and actuated using a rack-and-pinion mechanism driven by a Dynamixel motor. Adhesive is delivered through a flexible tube to a needle located at the end-effector. The sleeve installer is a compact gripper equipped with a locking mechanism that holds and aligns the sleeve, releasing it onto the pipe upon triggering.

C. System Integration

As shown in Fig. 3, the developed UAM integrates a Pixhawk 6C running PX4 for low-level flight control and an onboard IMU fused with Intel RealSense T265 visual–inertial odometry through PX4's Extended Kalman Filter for state estimation. High-level perception and control are handled by an NVIDIA Jetson Nano running Ubuntu and ROS, which communicates with the Pixhawk via MAVLink and drives five Dynamixel actuators through a U2D2 TTL interface. Remote operation is achieved through a ROS-based ground station over Wi-Fi.

Power is supplied by a 4S 14.8 V LiPo battery via a power distribution board (PDB) and a power module. The 14.8 V line feeds four ESCs for the brushless motors, and two DC–DC converters regulate 5 V for the Jetson Nano and Dynamixel actuators.

For simulation, the same configuration is modeled using equivalent parameters and component placement to match the total mass and dynamic characteristics of the prototype. These assumptions ensure that the simulated behavior closely reflects the real system's dynamics and control performance.

D. Coordinate Frames and System Configuration

To describe the system configuration, four coordinate frames are defined: the world frame (I), the UAV body frame

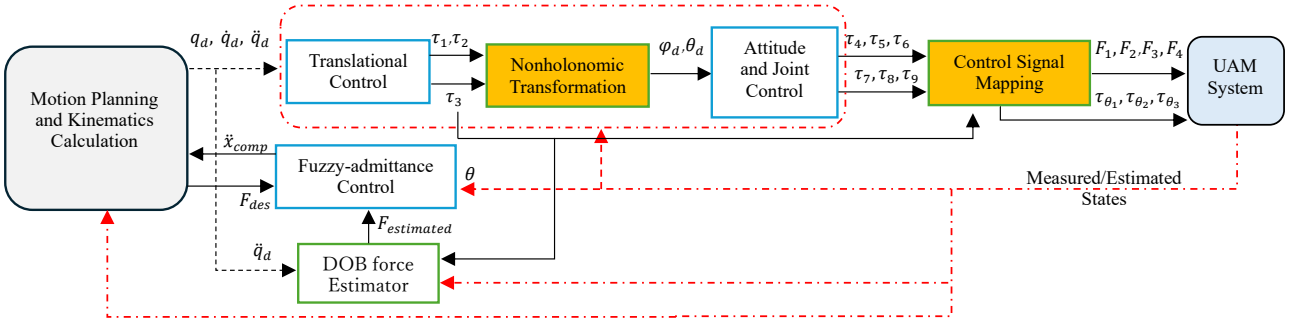

Fig. 4. The proposed unified control for the UAM system

(*B*), the manipulator base frame (*M*), and the end-effector frame (*E*), as shown in Fig. 2. The full set of generalized coordinates for the UAM is defined as

$$q = [x,\ y,\ z,\ \phi,\ \theta,\ \psi,\ \theta_1,\ \theta_2,\ \theta_3]^\top \in \mathbb{R}^9, \tag{1}$$

where $[x, y, z]^\top \in \mathbb{R}^3$ represent the UAV position in frame *I*, $[\phi, \theta, \psi]^\top \in \mathbb{R}^3$ are the roll, pitch, and yaw angles, and $[\theta_1, \theta_2, \theta_3]^\top \in \mathbb{R}^3$ are the joint angles of the manipulator, each defined as a clockwise rotation about the negative z-axis of *M*. For control design, q is partitioned into

$$q_p = [x,\ y,\ z]^\top \in \mathbb{R}^3, \quad q_a = [\phi,\ \theta,\ \psi,\ \theta_1,\ \theta_2,\ \theta_3]^\top \in \mathbb{R}^6.$$

IV. Trajectory Controller

The control framework integrates inner-loop controllers for translation, attitude, and joints, based on AB and AFTSMC, as shown in Fig. 4.

A. Translation Control via AB

To regulate the UAM's translational motion, the AB controller operates on the position subsystem $q_p \in \mathbb{R}^3$. Let the position tracking error be defined as $e_1 = q_p - q_{p,d} \in \mathbb{R}^3$, and the augmented error as $e_2 = \dot{e}_1 + \alpha e_1 \in \mathbb{R}^3$, where $\alpha > 0$ is a control gain. A virtual control input $\nu \in \mathbb{R}^3$ is then designed as

$$\nu = \ddot{q}_{p,d} - \alpha\dot{e}_1 - \gamma e_2 - e_1, \tag{2}$$

where $\gamma > 0$ is a scalar gain. The calculated translational torque $\tau_p = [\tau_1, \tau_2, \tau_3]^\top \in \mathbb{R}^3$ is computed as

$$\tau_p = \hat{M}_p\nu + \hat{C}_p\dot{q}_p + \hat{G}_p + \hat{\Xi}_p, \tag{3}$$

where $\hat{M}_p \in \mathbb{R}^{3\times3}$, $\hat{C}_p \in \mathbb{R}^{3\times3}$, and $\hat{G}_p \in \mathbb{R}^3$ denote the translational components of the nominal inertia, Coriolis, and gravity matrices, respectively. These components are derived using the Lagrange method [23]. The vector $\hat{\Xi}_p \in \mathbb{R}^3$ represents an adaptive estimate of the lumped disturbances, including uncertainties and external forces. This estimate is updated online using the adaptation law $\dot{\hat{\Xi}}_p = -\beta e_2$, where $\beta > 0$ is the adaptive gain.

The τ_p obtained from (3) is used to compute ϕ_d and θ_d through a nonholonomic transformation as follows

$$\begin{bmatrix}\theta_d\\ \phi_d\end{bmatrix} = \frac{1}{\tau_3}\begin{bmatrix}\cos\psi & \sin\psi\\ \sin\psi & -\cos\psi\end{bmatrix}\begin{bmatrix}\tau_1\\ \tau_2\end{bmatrix}. \tag{4}$$

This relationship reflects the UAV's underactuated nature, where horizontal position tracking is achieved via attitude modulation, and the resulting desired angles are passed to the attitude controller.

B. Attitude and Joint Control via AFTSMC

The AFTSMC is applied to control the UAV attitude and manipulator joints. The sliding surface is defined as

$$s = \dot{e} + \lambda e_{\text{reg}}^{r/\eta}\,\text{sign}(e), \tag{5}$$

where $e = q_a - q_{a,d} \in \mathbb{R}^6$, $\lambda > 0$ is the sliding gain, and $r, \eta > 0$ satisfy $0 < \frac{r}{\eta} < 1$. The regularized error is $e_{\text{reg}} = \max(|e|, \varepsilon)$, with small $\varepsilon > 0$, to prevent singularities near zero. Hence, the virtual control input $v \in \mathbb{R}^6$ is then defined as

$$v = \ddot{q}_{a,d} - \lambda\left(\frac{r}{\eta}\,e_{\text{reg}}^{\frac{r}{\eta}-1}\,\dot{e}\right), \tag{6}$$

The control law combines equivalent dynamics compensation and a super-twisting-based reaching law, and is expressed as

$$\tau_a = \hat{M}_a v + \hat{C}_a\dot{q}_a + \hat{G}_a + \hat{\Xi}_a + u, \tag{7}$$

where $\tau_a = [\tau_4,\ \tau_5,\ \tau_6,\ \tau_7,\ \tau_8,\ \tau_9]^\top \in \mathbb{R}^6$ denotes the attitude–joint control inputs. The matrices $\hat{M}_a \in \mathbb{R}^{6\times6}$, $\hat{C}_a \in \mathbb{R}^{6\times6}$, and the vector $\hat{G}_a \in \mathbb{R}^6$ represent the nominal attitude–joint dynamics. Here, u is the integral action from the super-twisting reaching law, and $\hat{\Xi}_a \in \mathbb{R}^6$ is an adaptive estimate of lumped disturbances. The estimate is updated online using the adaptation law $\dot{\hat{\Xi}}_a = -\zeta s$, where $\zeta > 0$ is the adaptive gain.

This modular framework demonstrates rapid convergence, mitigates chattering effects, and supports computationally efficient real-time implementation on onboard processors.

V. Fuzzy-Admittance-Based Compliant Force Control Strategy

This section presents a fuzzy-admittance control strategy for achieving indirect and compliant force interaction in aerial manipulation. By leveraging force–dynamic awareness, the controller adjusts the quadrotor's pitch angle θ to indirectly generate contact forces, promoting stable end-effector contact during tasks such as sleeve installation. The approach adapts to dynamic changes and supports smooth

buildup and stable disengagement of contact forces with minimal overshoot or oscillation.

A. Force Generation via Pitch Modulation

The quadrotor generates horizontal contact force by tilting its body through θ. Assuming the thrust is aligned with the body-Z-axis and neglecting aerodynamic effects, the horizontal contact force F can be approximated as

$$F \approx m_{eq} g \tan(\theta), \tag{8}$$

where m_{eq} is the equivalent mass of the system including the payload, and g is gravitational acceleration. This yields the theoretical pitch angle required to generate a specified contact force, which is then used to configure the parameter bounds of the fuzzy membership functions.

B. Fuzzy Logic Controller Design

A Mamdani-type fuzzy logic controller is implemented with two inputs: the force error $F_{\text{e}} = F_{\text{des}} - F_{\text{estimated}}$ and the measured θ, and one output: the compliant acceleration $\ddot{x}_{\text{comp}}$. Triangular membership functions are used for all variables, with linguistic terms Negative Large (NL), Negative Small (NS), Zero (Z), Positive Small (PS), Positive Medium (PM), and Positive Large (PL). The membership terms and variable ranges are summarized in Table I. These terms qualitatively describe the variable magnitudes and directions, ranging from strong negative to strong positive. The controller employs a min–max inference rule base with centroid defuzzification to produce an acceleration command, which is integrated to obtain the compliant velocity $\dot{x}_{\text{comp}}$ and displacement Δx_{comp} as shown in Fig. 4.

The fuzzy logic controller contributes to tracking the desired contact force by generating compliant acceleration commands. For large force errors F_{error} (e.g., PL or NL), the controller outputs a high acceleration to accelerate convergence. However, as the pitch angle θ increases, the effective inertia of the UAM in the horizontal direction also grows due to dynamic coupling. To compensate, the rule base progressively reduces the output; for example, if F_{error} is positive and θ shifts from PS to PM or PL, the output transitions from PS to NS or NL, slowing forward motion and preventing overshoot. Near-zero errors or small θ yield near-zero outputs, stabilizing the contact. This design promotes smooth force buildup, stable holding, and compliant adaptation under changing inertia and contact dynamics.

C. World-Frame Mapping for Force Direction Alignment

The fuzzy controller computes the compliant acceleration $\ddot{x}_{\text{comp}}$ in the horizontal projection of the quadrotor's body-x axis. To generate a compliant force along the direction of an arbitrarily oriented pipe in 2D, the quadrotor performs yaw alignment such that its body-x axis aligns with the pipe orientation angle ψ, then performs the interaction. The compliant acceleration is then mapped into the world frame as

$$\begin{bmatrix} \ddot{x}_d \\ \ddot{y}_d \end{bmatrix} = \ddot{x}_{\text{comp}} \begin{bmatrix} \cos\psi \\ \sin\psi \end{bmatrix}. \tag{9}$$

TABLE I
FUZZY LOGIC CONTROLLER PARAMETERS

Variable	Membership Terms	Range
F_e	NL, NS, Z, PS, PL	[–2, 2] N
θ	Z, PS, PM, PL	[0,9] deg
$\ddot{x}_{\text{comp}}$	NL, NS, Z, PS, PL	[–0.003, 0.0045] m/s^2

The same transformation is applied to the integrated velocity and displacement vectors in the world frame. This approach enables compliant force control along any pipeline direction by dynamically aligning the quadrotor–manipulator system's response with the task direction defined by ψ.

D. Manipulator–Quadrotor Collaboration

As the quadrotor pitches to generate contact force, the attached manipulator base tilts, altering the end-effector pose in task space. To preserve the desired sleeve orientation in the world frame, the third joint compensates for this tilt as

$$\Delta\theta_{3,d} = -\theta, \tag{10}$$

where $\Delta\theta_{3,d}$ denotes the compensatory change in the third joint angle. This correction maintains stable contact geometry and task accuracy. A key advantage of the proposed manipulator is its decoupled motion structure: θ_3 regulates orientation, while θ_1 and θ_2 control planar positioning, enabling precise force interaction without trajectory distortion.

VI. SENSORLESS FORCE ESTIMATION USING A DISTURBANCE OBSERVER

In aerial manipulation, contact-aware control requires accurate estimation of interaction forces between the manipulator and the environment. Physical force sensors, however, add complexity, weight, and cost. To address this, a lightweight, computationally efficient sensorless force estimation method is implemented using a DOB. Operating in the world frame, it relies solely on onboard parameters: measured or estimated inputs (linear accelerations, attitude angles) and calculated quantities (controller thrust output, mass).

A. Estimation Principle in the World Frame

The core idea is to estimate the external forces acting on the UAM by comparing model-predicted and measured accelerations, attributing any discrepancy to unmodeled disturbances, such as contact forces. The formulation is expressed in the world frame (*I*) for consistent transformation into the UAV body and end-effector frames, ensuring applicability to manipulation tasks with arbitrary orientations.

The model-predicted acceleration represents the nominal motion expected from the trajectory commands and system dynamics in the absence of external forces, combining the desired accelerations $\ddot{q}_{d,i}$ from the motion planner with those generated by the thrust vector and attitude. Accordingly, the model-predicted accelerations in frame *I* are computed as

$$\ddot{q}_i^{\text{model}} = \begin{cases} \ddot{q}_{d,x} + \dfrac{\tau_3}{m_{eq}} \dfrac{[R_b]_{(1,3)}}{[R_b]_{(3,3)}}, & i = x, \\ \ddot{q}_{d,y} + \dfrac{\tau_3}{m_{eq}} \dfrac{[R_b]_{(2,3)}}{[R_b]_{(3,3)}}, & i = y, \\ \dfrac{\tau_3}{m_{eq}} - g, & i = z, \end{cases} \tag{11}$$

where R_b is the body-to-world rotation matrix derived from the Euler angles, and τ_3 represents the thrust command computed by the AB controller for vertical motion.

The raw external force estimate along each axis is then obtained as

$$F_i^{\text{raw}} = m_{eq}\left(\ddot{q}_i^{\text{meas}} - \ddot{q}_i^{\text{model}}\right), \quad i \in \{x, y, z\}, \tag{12}$$

where $\ddot{q}_i^{\text{meas}}$ is the measured or estimated translational acceleration from onboard sensors expressed in frame *I*.

B. Filtering and Smoothing

To reduce measurement noise and provide a smooth external force signal suitable for compliant control or contact detection, F_i^{raw} is filtered using a first-order low-pass filter as

$$\hat{F}_i[n] = \hat{F}_i[n-1] + \kappa\left(F_i^{\text{raw}}[n] - \hat{F}_i[n-1]\right), \tag{13}$$

where $\hat{F}_i[n]$ is the filtered force and $\kappa \in (0, 1)$ is the smoothing coefficient. The coefficient κ is defined in terms of the cutoff frequency ω_c and the sampling interval dt as

$$\kappa = \frac{\omega_c \cdot dt}{1 + \omega_c \cdot dt}. \tag{14}$$

C. Frame Transformations

The estimated external force vector expressed in frame *I* is then given by

$$\hat{\mathbf{F}}_{\text{world}} = \begin{bmatrix}\hat{F}_x & \hat{F}_y & \hat{F}_z\end{bmatrix}^\top, \tag{15}$$

where $\hat{F}_x, \hat{F}_y$, and $\hat{F}_z$ denote the estimated force components along the x-, y-, and z-axes, respectively. To express the estimated force in frame *B*, a rotation transformation is applied as

$$\hat{\mathbf{F}}_{\text{body}} = R_b^\top \hat{\mathbf{F}}_{\text{world}}, \tag{16}$$

Finally, the estimated force at the end-effector frame *E* is obtained as

$$\hat{\mathbf{F}}_{\text{ee}} = R_{\text{ee}}^\top \hat{\mathbf{F}}_{\text{body}}, \quad R_{\text{ee}} = R_y\left(\tfrac{3\pi}{2} - \theta_3\right), \tag{17}$$

where R_{ee} represents the rotation from frame *E* to frame *B*, accounting for θ_3. A pure rotational transformation is used since the DOB estimates only forces, not full wrenches.

This modular formulation allows projection of external forces to the end-effector frame for task-space interpretation and compliant interaction under varying orientations. The lightweight observer reduces reliance on differentiation and full-state estimation, supporting real-time implementation for onboard aerial manipulation.

To initiate fuzzy force control autonomously, the motion planner monitors the end-effector position via forward kinematics and compares it with the target crack location. When the tip enters a predefined tolerance zone and the DOB-estimated external force indicates contact, a trigger flag activates the fuzzy controller to enable compliant interaction. The integration of the DOB within the control system is illustrated in Fig. 4.

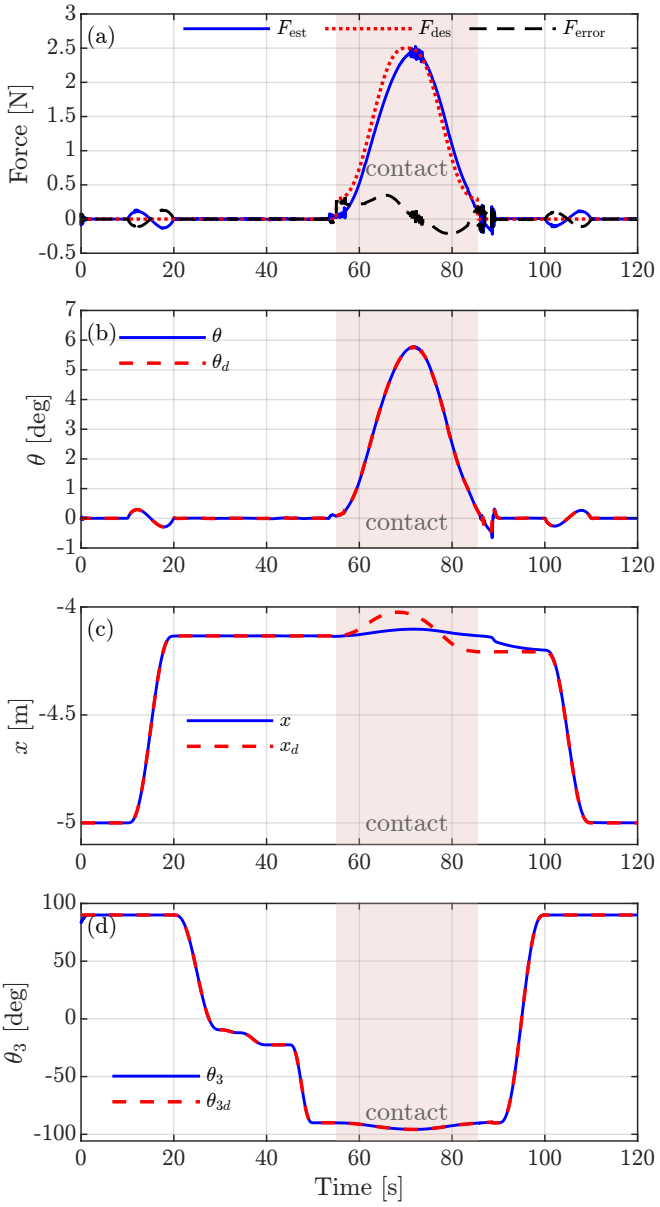

Fig. 5. Tracking performance: (a) contact force response, (b) pitch angle θ, (c) translational position x, and (d) manipulator joint angle θ_3.

VII. 3D Simulation Experiments and Results

This section presents the evaluation of the proposed unified control and force estimation strategy using a MATLAB/Simscape physics-based simulation [29].

A. Setup

The experiment begins with autonomous takeoff and trajectory tracking toward the predefined crack location. Once aligned, the system performs two repair steps: first, adhesive is dispensed along the pipe surface, simulated as a trajectory around the circumference; second, the manipulator reorients to position the sleeve tool and initiates contact. To model sleeve–pipe interaction, contact forces were applied between the inner sleeve surface and outer pipe surface, with stiffness 50×10^3 N/m and damping 50 N·s/m to represent a rigid pipe. High friction due to the adhesive was modeled with static

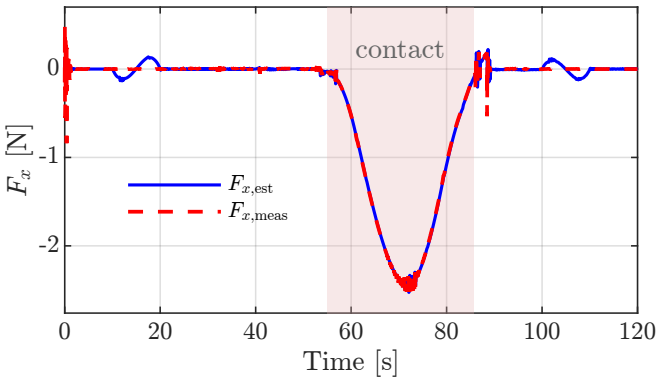

Fig. 6. Force estimation validation in the x-direction: comparison between the estimated and measured contact forces, with the contact phase highlighted.

TABLE II

ROOT MEAN SQUARE ERROR (RMSE) RESULTS

Force Tracking and Estimation

Comparison	RMSE
F_x^{est} vs F_x^{des}	0.2093 N
F_x^{meas} vs F_x^{des}	0.2038 N
F_x^{est} vs F_x^{meas}	0.0397 N

State Tracking

State	RMSE	Joint	RMSE
x	0.0312 m	θ_1	0.0247 deg
y	0.0001 m	θ_2	0.1632 deg
z	0.0015 m	θ_3	0.3286 deg
ϕ	0.0038 deg		
θ	0.0272 deg		
ψ	0.0071 deg		

and dynamic friction coefficients $\mu_s = 1.0$ and $\mu_k = 0.9$, respectively. The sleeve mass was set to 0.1 kg. At the contact stage, the fuzzy–admittance controller regulates the contact force, following a quintic reference profile that ramps smoothly to 2.5 N, representing the sleeve sealing process.

B. Results

Fig. 5(a) shows the desired and estimated contact forces. Since the applied force is compressive, it is plotted with an inverted sign (-1) for clarity. The results show a gradual build-up of force as θ increases (Fig. 5(b)), beginning with a small positive bias of 0.3 N to ensure consistent contact and mitigate mismatches or initial estimator spikes. Fig. 5(c) illustrates the translational position x, where a deviation arises at contact from virtual displacement. This deviation generates the contact force while the controller works to reduce the tracking error. In Fig. 5(d), the manipulator joint θ_3 accurately follows its desired trajectory, compensating for the quadrotor's inclination to maintain correct sleeve orientation at the crack location.

While the estimated force does not perfectly follow the quintic reference due to quadrotor underactuation and the difficulty of replicating gradual ramps, the results remain reasonable. Importantly, the controller achieves not only compliant force build-up but also smooth force reduction before releasing the sleeve. This backward reduction phase

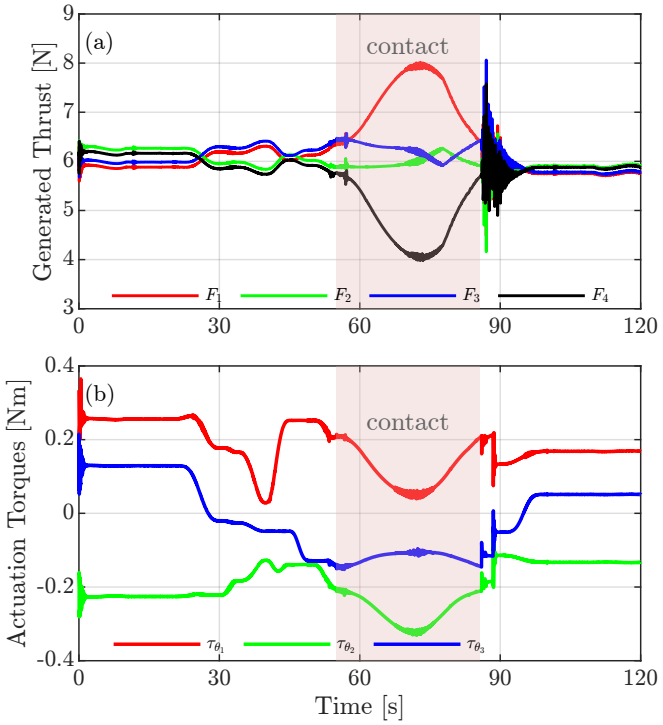

Fig. 7. Motors outputs: (a) generated thrust of the quadrotor, and (b) actuation torques of the manipulator.

is critical for returning θ to its nominal value without inducing oscillations or collisions. Validation of the force estimator against measured reaction forces at the end-effector joint, as shown in Fig. 6, confirms accurate tracking during contact. In free flight, the DOB registers small apparent forces from minor mismatches between desired and actual accelerations, which are filtered using a contact-detection condition based on the end-effector's proximity to the crack location discussed in the previous section.

Quantitatively, Table II summarizes the root mean square error (RMSE) values for force tracking and state estimation. During contact, the RMSE between estimated and measured force is 0.0397 N, while relative to the desired force it is 0.2093 N (estimated) and 0.2038 N (measured). The nine system states also exhibit consistent performance: in the x-direction, the RMSE is 0.0312 m, reflecting a small deviation from the virtual displacement during contact that reduces after the controller recovers following sleeve release. The RMSE along the y-axis remains nearly zero, since motion and interaction occur primarily along x, while the z-axis error is limited to 0.0015 m, indicating minimal altitude variation. Orientation RMSEs stay below 0.03°, and joint angles within 0.4°. These results suggest that the proposed unified trajectory and fuzzy-admittance control framework provides accurate tracking and compliant force regulation in simulation.

Finally, Fig. 7 presents the motor thrusts and actuator torques. Variations observed during sleeve release, resulting from payload change and the end of contact between the sleeve and end-effector, are regarded as disturbances and handled by the controller. All output signals remain within

the datasheet limits: thrusts below 13 N [27] and torques below 0.93 Nm [28], indicating feasible operation for real-world implementation.

VIII. Conclusion

This study presents a unified control framework that achieves robust trajectory tracking and force-compliant behavior for aerial manipulators performing contact-based tasks. By integrating a fuzzy-admittance outer loop with an AB–AFTSMC inner loop, the system demonstrates stable interaction force regulation while maintaining high-precision motion tracking. The fuzzy logic controller adapts to pitch-induced dynamic variations, and the lightweight DOB provides real-time, sensorless force estimation without requiring physical sensors. Force control is activated based on estimated contact and end-effector position, supporting smooth transitions between free flight and physical interaction.

Overall, this work contributes toward intelligent, force-aware aerial manipulation by combining dynamic adaptability with computational efficiency. The proposed framework is applicable to tasks requiring compliant interaction, such as infrastructure maintenance, precision assembly, and sensor installation. Future work will focus on experimental validation using the developed prototype and on refining the control algorithms to handle real-world disturbances, including aerodynamic effects, sensor noise, and communication delay. Additional efforts will enhance the fuzzy controller through AI-based reasoning and refine the DOB to distinguish between classes of external forces and disturbances, enabling more context-aware and autonomous aerial interaction.

References

[1] Q. Lindsey, D. Mellinger, and V. Kumar, "Construction with quadrotor teams," *Autonomous Robots*, vol. 33, no. 3, pp. 323–336, 2012.

[2] M. Kamezaki, M. Miyata, and S. Sugano, "Video presentation based on multiple-flying camera to provide continuous and complementary images for teleoperation," *Automation in Construction*, vol. 159, p. 105285, 2024.

[3] D. Mellinger, Q. Lindsey, M. Shomin, and V. Kumar, "Design, modeling, estimation, and control for aerial grasping and manipulation," in *2011 IEEE/RSJ International Conference on Intelligent Robots and Systems*, pp. 2668–2673, IEEE, 2011.

[4] H. Seo, S. Kim, and H. J. Kim, "Aerial grasping of cylindrical object using visual servoing based on stochastic model predictive control," in *2017 IEEE international conference on robotics and automation (ICRA)*, pp. 6362–6368, IEEE, 2017.

[5] M. Schuster, D. Bernstein, P. Reck, S. Hamaza, and M. Beitelschmidt, "Automated aerial screwing with a fully actuated aerial manipulator," in *2022 IEEE/RSJ International Conference on Intelligent Robots and Systems (IROS)*, pp. 3340–3347, IEEE, 2022.

[6] K. Zhang, P. Chermprayong, F. Xiao, D. Tzoumanikas, B. Dams, S. Kay, B. B. Kocer, A. Burns, L. Orr, T. Alhinai, *et al.*, "Aerial additive manufacturing with multiple autonomous robots," *Nature*, vol. 609, no. 7928, pp. 709–717, 2022.

[7] A. Jimenez-Cano, J. Braga, G. Heredia, and A. Ollero, "Aerial manipulator for structure inspection by contact from the underside," in *2015 IEEE/RSJ international conference on intelligent robots and systems (IROS)*, pp. 1879–1884, IEEE, 2015.

[8] M. Tognon, H. A. T. Chávez, E. Gasparin, Q. Sablé, D. Bicego, A. Mallet, M. Lany, G. Santi, B. Revaz, J. Cortés, *et al.*, "A truly-redundant aerial manipulator system with application to push-and-slide inspection in industrial plants," *IEEE Robotics and Automation Letters*, vol. 4, no. 2, pp. 1846–1851, 2019.

[9] R. Batisse, "Review of gas transmission pipeline repair methods," in *Safety, reliability and risks associated with water, oil and gas pipelines*, pp. 335–349, Springer, 2008.

[10] P. Chermprayong, K. Zhang, F. Xiao, and M. Kovac, "An integrated delta manipulator for aerial repair: A new aerial robotic system," *IEEE Robotics & Automation Magazine*, vol. 26, no. 1, pp. 54–66, 2019.

[11] E. N. Moustafa, M. Kamezaki, A. Khalifa, S. Miyake, T. Miyake, and S. Sugano, "Development of a two-dof three-parallelogram aerial manipulator for pipeline crack repair using a two-tool end-effector and onboard sensor-based localization," in *2025 IEEE/ASME International Conference on Advanced Intelligent Mechatronics (AIM)*, pp. 1–7, IEEE, 2025.

[12] X. Meng, Y. He, and J. Han, "Survey on aerial manipulator: System, modeling, and control," *Robotica*, vol. 38, no. 7, pp. 1288–1317, 2020.

[13] T. Tomić, C. Ott, and S. Haddadin, "External wrench estimation, collision detection, and reflex reaction for flying robots," *IEEE Transactions on Robotics*, vol. 33, no. 6, pp. 1467–1482, 2017.

[14] K. Bodie, M. Brunner, M. Pantic, S. Walser, P. Pfändler, U. Angst, R. Siegwart, and J. Nieto, "An omnidirectional aerial manipulation platform for contact-based inspection," *arXiv preprint arXiv:1905.03502*, 2019.

[15] B. Stephens, H.-N. Nguyen, S. Hamaza, and M. Kovac, "An integrated framework for autonomous sensor placement with aerial robots," *IEEE/ASME Transactions on Mechatronics*, vol. 28, no. 1, pp. 38–49, 2022.

[16] S. Bellens, J. De Schutter, and H. Bruyninckx, "A hybrid pose/wrench control framework for quadrotor helicopters," in *2012 IEEE International Conference on Robotics and Automation*, pp. 2269–2274, IEEE, 2012.

[17] S. Hamaza, I. Georgilas, M. Fernandez, P. Sanchez, T. Richardson, G. Heredia, and A. Ollero, "Sensor installation and retrieval operations using an unmanned aerial manipulator," *IEEE Robotics and Automation Letters*, vol. 4, no. 3, pp. 2793–2800, 2019.

[18] H. W. Wopereis, J. J. Hoekstra, T. H. Post, G. A. Folkertsma, S. Stramigioli, and M. Fumagalli, "Application of substantial and sustained force to vertical surfaces using a quadrotor," in *2017 IEEE international conference on robotics and automation (ICRA)*, pp. 2704–2709, IEEE, 2017.

[19] E. Sariyildiz, "A guide to design disturbance observer-based motion control systems in discrete-time domain," in *2021 IEEE International Conference on Mechatronics (ICM)*, pp. 1–6, IEEE, 2021.

[20] C. D. McKinnon and A. Schoellig, "Unscented external force and torque estimation for quadrotors. in 2016 ieee," in *RSJ International Conference on Intelligent Robots and Systems (IROS)*, pp. 5651–5657.

[21] A. Khalifa, M. Fanni, and A. Khalifa, "Sensorless contact force estimation and robust impedance control for a quadrotor manipulation system," *Scientific Reports*, vol. 14, no. 1, p. 28772, 2024.

[22] D. Lee, H. Seo, D. Kim, and H. J. Kim, "Aerial manipulation using model predictive control for opening a hinged door," in *2020 IEEE International Conference on Robotics and Automation (ICRA)*, pp. 1237–1242, 2020.

[23] S. Kim, S. Choi, and H. J. Kim, "Aerial manipulation using a quadrotor with a two dof robotic arm," in *2013 IEEE/RSJ International Conference on Intelligent Robots and Systems*, pp. 4990–4995, IEEE, 2013.

[24] Y. Chen, J. Liang, Y. Wu, Z. Miao, H. Zhang, and Y. Wang, "Adaptive sliding-mode disturbance observer-based finite-time control for unmanned aerial manipulator with prescribed performance," *IEEE transactions on cybernetics*, vol. 53, no. 5, pp. 3263–3276, 2022.

[25] J. Liang, Y. Chen, Y. Wu, Z. Miao, H. Zhang, and Y. Wang, "Adaptive prescribed performance control of unmanned aerial manipulator with disturbances," *IEEE Transactions on Automation Science and Engineering*, vol. 20, no. 3, pp. 1804–1814, 2022.

[26] J. Liang, Y. Chen, N. Lai, B. He, Z. Miao, and Y. Wang, "Low-complexity prescribed performance control for unmanned aerial manipulator robot system under model uncertainty and unknown disturbances," *IEEE Transactions on Industrial Informatics*, vol. 18, no. 7, pp. 4632–4641, 2021.

[27] Holybro, "Px4 development kit x500 v2." `https://holybro.com/collections/multicopter-kit/products/px4-development-kit-x500-v2`, 2025. Accessed: 2025-05-15.

[28] ROBOTIS, "Dynamixel xc330-m288-t e-manual." `https://emanual.robotis.com/docs/en/dxl/x/xc330-m288/`, 2025. Accessed: 2025-05-18.

[29] MathWorks, "Quadcopter package delivery." `https://www.mathworks.com/help/sm/ug/quadcopter.html`, 2024. Accessed: 2025-05-18.